Journal of
Biomedical Optics

BiomedicalOptics.SPIEDigitalLibrary.org

Swept-source optical coherence tomography powered by a 1.3-μm vertical cavity surface emitting laser enables 2.3-mm-deep brain imaging in mice *in vivo*

Woo June Choi
Ruikang K. Wang

SPIE.

Journal of Biomedical Optics 20(10), 106004 (October 2015)

Swept-source optical coherence tomography powered by a 1.3-μm vertical cavity surface emitting laser enables 2.3-mm-deep brain imaging in mice *in vivo*

Woo June Choi and Ruikang K. Wang*
University of Washington, Department of Bioengineering, 3720 15th Avenue NE, Seattle, Washington 98195, United States

Abstract. We report noninvasive, *in vivo* optical imaging deep within a mouse brain by swept-source optical coherence tomography (SS-OCT), enabled by a 1.3-μm vertical cavity surface emitting laser (VCSEL). VCSEL SS-OCT offers a constant signal sensitivity of 105 dB throughout an entire depth of 4.25 mm in air, ensuring an extended usable imaging depth range of more than 2 mm in turbid biological tissue. Using this approach, we show deep brain imaging in mice with an open-skull cranial window preparation, revealing intact mouse brain anatomy from the superficial cerebral cortex to the deep hippocampus. VCSEL SS-OCT would be applicable to small animal studies for the investigation of deep tissue compartments in living brains where diseases such as dementia and tumor can take their toll. [DOI: 10.1117/1.JBO.20.10.106004]

Keywords: deep brain imaging in mouse brain; vertical cavity surface emitting laser; swept-source optical coherence tomography.

Paper 150453LRR received Jul. 2, 2015; accepted for publication Sep. 15, 2015; published online Oct. 8, 2015.

1 Introduction

Optical coherence tomography (OCT) is a noninvasive optical imaging technology that provides micrometer-resolution cross-sectional images of subsurface tissue microstructure.[1] Over the past decades, advances in OCT technology have enabled intense expansion of its application to a variety of biomedical fields, encompassing both basic science and clinical investigations.[1] In particular, the use of OCT in neuroscience holds promise in the investigation of small animal brains *in vivo*. Several research groups have demonstrated OCT imaging to visualize structure, neural activity, and hemodynamics in the cerebral cortex of a mouse model *in vivo*.[2–4] This OCT brain imaging has assisted preclinical studies on brain disorders, such as experimental ischemic stroke, traumatic brain injury, and brain tumor.

Despite the potential demonstrations in brain research, current OCT brain studies have been limited to the cortical layer within mouse brain. Apart from strong light scattering by heterogeneous brain tissue, one possible underlying reason that the existing OCT is not capable of visualizing brain tissue compartments below the cortex (located at >1 mm below the brain surface in adult mice) is in its significant limitation of maximal imaging depth range. This is due to the progressive dropoff over −10 dB in sensitivity at larger depth (typically, >1 mm from a zero delay line), which is an inherent challenge for conventional Fourier-domain OCT systems. The sensitivity degradation precludes OCT from imaging subcortical tissue compartments such as the hippocampus where many pathologies originate.

Recently, swept-source OCT (SS-OCT) powered by a MEMS-tunable vertical cavity surface emitting laser (VCSEL) has shown dramatic improvement in its usable imaging range.[5] The single longitudinal mode operation of VCSELs generates a very narrow spectral linewidth, supporting a long coherence length of more than 100 mm.[5] Therefore, the OCT signal sensitivity remains almost constant with nominal dropoff at distances in excess of several millimeters. With a limited bandwidth of data acquisition electronics, VCSEL SS-OCT was able to offer longer imaging depths than have been commonly achieved to date.[5,6] This markedly extended depth would open up new opportunities to fulfill a number of imaging scenarios that have barely been attempted in the OCT community, such as full-length imaging of a human eye from cornea to retina.[6]

In this letter, we report one potential use of VCSEL SS-OCT for deep brain imaging in living small animals. An adult mouse brain is imaged with a VCSEL SS-OCT system through an open-skull cranial window. The imaging result is compared with that of a conventional SS-OCT system, showing the superior imaging capability of the proposed approach for deep brain imaging and revealing the structural anatomy of the cerebral cortex and subcortex *in vivo*.

2 Materials and Methods

2.1 *Vertical Cavity Surface Emitting Laser Swept-Source Optical Coherence Tomography System*

In this work, we used a 1.3-μm VCSEL SS-OCT system provided by Thorlabs (OCS1310V1, Thorlabs, Inc. Newton, New Jersey) for deep brain imaging.[7] The system layout is illustrated in Fig. 1. A MEMS tunable VCSEL was used as the OCT light source, sweeping lasing wavelengths at 100 kHz across a broad spectral range of 100 nm (−10 dB) centered at 1.3 μm.[7] A small portion of the output beam from the VCSEL laser cavity module

---

*Address all correspondence to: Ruikang K. Wang, E-mail: wangrk@uw.edu

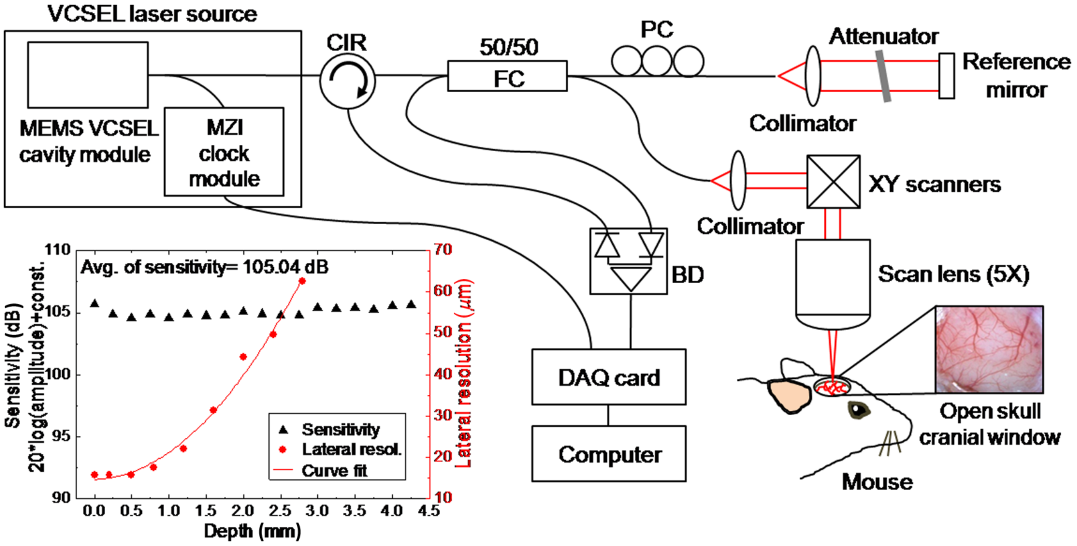

Fig. 1 Schematic of the 1.3-μm vertical cavity surface emitting laser (VCSEL) swept-source optical coherence tomography (SS-OCT) system. MZI, Mach–Zehnder interferometer; CIR, circulator; FC, optical fiber coupler; PC, polarization controller; BD, dual balanced detector; DAQ, data acquisition. The inset graph shows the sensitivity profile and the lateral resolutions, measured along a depth scan.

was launched into a Mach–Zehnder interferometer (MZI) clock module to achieve real-time optical clocking, upon which OCT spectral fringes can be evenly sampled in wavenumbers with the referenced MZI signals, eliminating the necessity of postprocessing for fringe resampling. The rest of the output beam was coupled into a main OCT interferometer, consisting of a circulator (CIR), a 50/50 optical fiber coupler, a reference arm, and a sample arm including a pair of XY galvo mirrors and a 5× OCT scan lens (LSM03, N.A. = 0.055, W.D. = 25.1 mm, Thorlabs, Inc.). The interferogram was detected by a dual balanced detector and then linearly sampled by a 12 bit, 500 MS/s data acquisition card. Thus, the depth-dependent reflectivity profile (A-line) was produced by fast Fourier transformation of the sampled fringe signals. The OCT volume dataset of the sample could be generated by fast (B-scan) and slow axis scanning (C-scan) using the XY galvo mirrors in the sample arm.

To measure system sensitivity, A-line OCT signals of a well-calibrated 40-dB attenuator were captured by varying the optical delay of the reference arm, and then the peaks of their point spread functions were located from each A-line. Sensitivity was calculated as the ratio of the peaks to the standard deviation of background noise. Lateral resolution in depth was measured by identifying minimal resolvable lines on *en-face* OCT images produced from a 1951 USAF resolution target (Edmund Optics, Barrington, New Jersey), moved down in the axial (Z) direction with step increments in a chamber filled with a liquid (alcohol). The refractive index of the liquid is 1.36, close to that of murine brain on average (1.35).[8] The inset graph in Fig. 1 shows the logarithmic sensitivity curve and lateral resolutions measured along different depths, where “0.0” of the depth (X axis) represents the zero-delay line for the sensitivity and a focal position for the lateral resolution. It is noted that the sensitivity is relatively constant with signal dropoff of only <1 dB from an average sensitivity value of 105.04 dB throughout an entire depth of 4.25 mm. Therefore, we speculate that the VCSEL SS-OCT system would promise an extended usable imaging depth range over a few millimeters for OCT imaging of turbid biological tissue such as a brain. However, degradation in the lateral

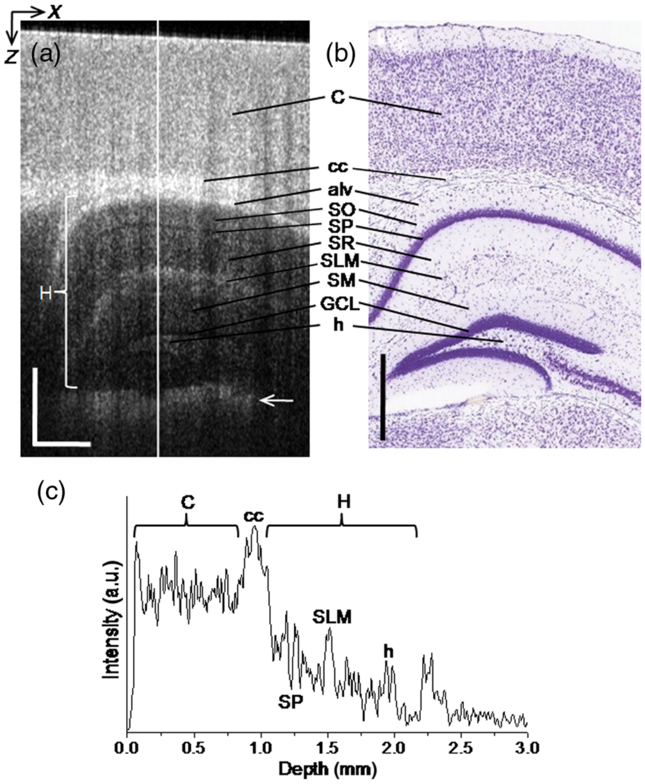

Fig. 2 *In vivo* 1.3-μm VCSEL SS-OCT imaging of a 12-week-old adult mouse with cranial window preparation. (a) Representative OCT image [2.5 mm (X) × 3.0 mm (Z)] at a coronal section of the mouse brain (2.3 mm posterior to bregma) under the cranial window, visualizing morphological details of the cerebral cortex and subsequent brain compartments. (b) This OCT brain anatomy shows good correlation with a photomicrograph of a Nissl-stained histology section of the same strain mouse brain (reprinted with a public courtesy from Allen Institute for Brain Science[12]). (c) Intensity profile taken at a marked white line in (a). C, cortex; cc, corpus callosum; H, hippocampus including alv, alveus of hippocampus; SO, stratum oriens; SP, stratum pyramidale; SR, stratum radiatum; SLM, stratum lacunosum-moleculare; SM, stratum moleculare; GCL, granule cell layer; h, hilus. Scale bar: 500 μm.

resolution was gradual from ~15 μm at 0.5 mm to ~50 μm at 2.4 mm behind the focus spot.

2.2 *Open-Skull Cranial Window Preparation*

We applied the traditional open-skull cranial window technique for the OCT probe beam to access mouse brain tissue. In preparation of the open-skull cranial window, three C57BL/6 mice (ages: 5 weeks to 12 weeks; weights: 23 to 25 g) were used in this study. The mice were anesthetized with a mixture of isoflurane (5% for induction, 1.5% during surgery and imaging), 0.2 L/ min O_2, and 0.8 L/ min air through a nose cone and then placed in prone position on a stereotaxic stage. A heating pad on the stereotaxic stage maintained the body temperature (~36.8°C) during the entire experiment. After disappearance of the toe pinching response, the skin and periosteum on top of the skull were removed. To create a cranial window, a circular groove was first thinned at the region of interest (1.0 mm posterior and lateral to bregma), located at the right parietal cortex, with a soft dental drill (Foredom Electric Co., Ethel, Connecticut). The groove was then slowly drilled with regular saline drops to avoid heating. After drilling, the cranium was gently lifted away from the skull with a pair of thin-tipped forceps and replaced with a 5-mm-diameter rounded cover slip (Thermo Scientific, Waltham, Massachusetts). The cover slip was sealed onto the skull with cyanoacrylate glue. Finally, a cranial window (4 × 4 mm) was made on the mouse brain with an available imaging area of ~3 × 3 mm. After the experiments, the animal was euthanized using 5% isoflurane overdose. All experimental animal procedures performed in this study were approved by the Institute of Animal Care and Use Committee (IACUC) of University of Washington (Protocol number: 4262-01).

3 Results

3.1 *In Vivo Deep Brain Imaging of Swept-Source Optical Coherence Tomography*

For VCSEL SS-OCT imaging, a 12-week-old adult mouse with cranial window preparation was placed under the OCT scan

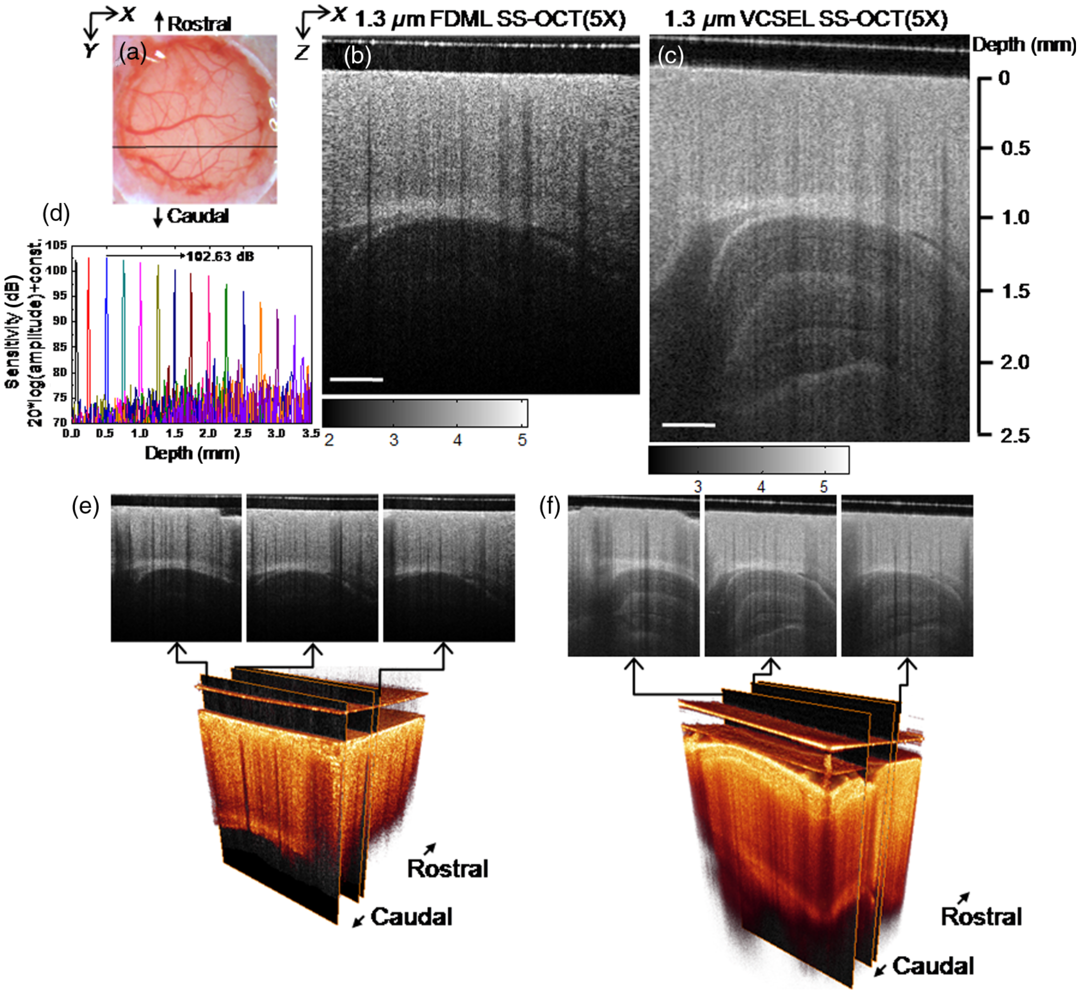

Fig. 3 Comparison of brain imaging between a 1.3-μm VCSEL SS-OCT system and a 1.3-μm Fourier-domain mode locking (FDML) SS-OCT system. A 5-week-old young adult mouse with cranial window preparation was used and sequentially imaged with two OCT systems under the same experimental conditions. (a) Bright-field microscope image of the cranial window. (b) FDML and (c) VCSEL SS-OCT images, obtained at the coronal section [solid line shown in (a)]. (d) Sensitivity roll-off curve of the FDML OCT system with 3-dB falling off at 2-mm depth. (e) and (f) show FDML and corresponding VCSEL SS-OCT cross-sections at different locations of the 3-D rendered brain structures in the cranial window, respectively. Scale bar: 500 μm.

lens. The position of the probe beam focal spot was properly adjusted around 500 μm below the brain surface with the aid of real-time ($\geq$80 frames/s) OCT B-mode display. The fluence of the incident beam was calculated as ~18.4 W/cm^2 for the 22-μm-diameter focal spot and the optical power of 7 mW well below the ANSI standards (~20 mW) for maximal allowed laser power at 1.3 μm.[9]

Figure 2(a) shows a representative OCT image [2.5 mm $(X) \times 3.0$ mm (Z)] at a coronal section of the mouse brain (2.3 mm posterior to bregma) below the cranial window. The imaging depth (Z) was rescaled with an average refractive index of murine brain cortex (1.35).[8] The OCT image allowed the brain to be observed in detail, consisting of characterized multilayers from the superficial cerebral cortex (C) to the deep hippocampal region (H) [Fig. 2(a)]. This brain morphology gave good correlation with a Nissl-stained coronal histology section of the same strain of mouse brain [Fig. 2(b)]. OCT signal broadening was prominent at the bottom of hippocampal region [arrow in Fig. 2(a)] due to the degradation of lateral resolution at the large depth. This issue may be mitigated by digital refocusing methods[10] or focus-engineering methods[11] through extending the depth of focus. Note that the shadows due to superficial blood vessels at the brain surface appear as vertically elongated black bars that traverse brain tissue layers in the OCT image. An intensity profile taken at a white line marked in Fig. 2(a) indicates that the 1.3-μm VCSEL SS-OCT delivers an imaging depth sufficient to include the 2.3-mm-deep brain tissue structure. Observation of brain structure beyond this depth would be extremely challenging because of significant attenuation of the light intensity due to the accumulation of multiple scattering events through the heterogeneous brain tissues.

3.2 Comparison of Deep Brain Imaging with a Conventional Swept-Source Optical Coherence Tomography System

The extended imaging ability for deep brain imaging was compared with a different type of 1.3-μm SS-OCT system using a

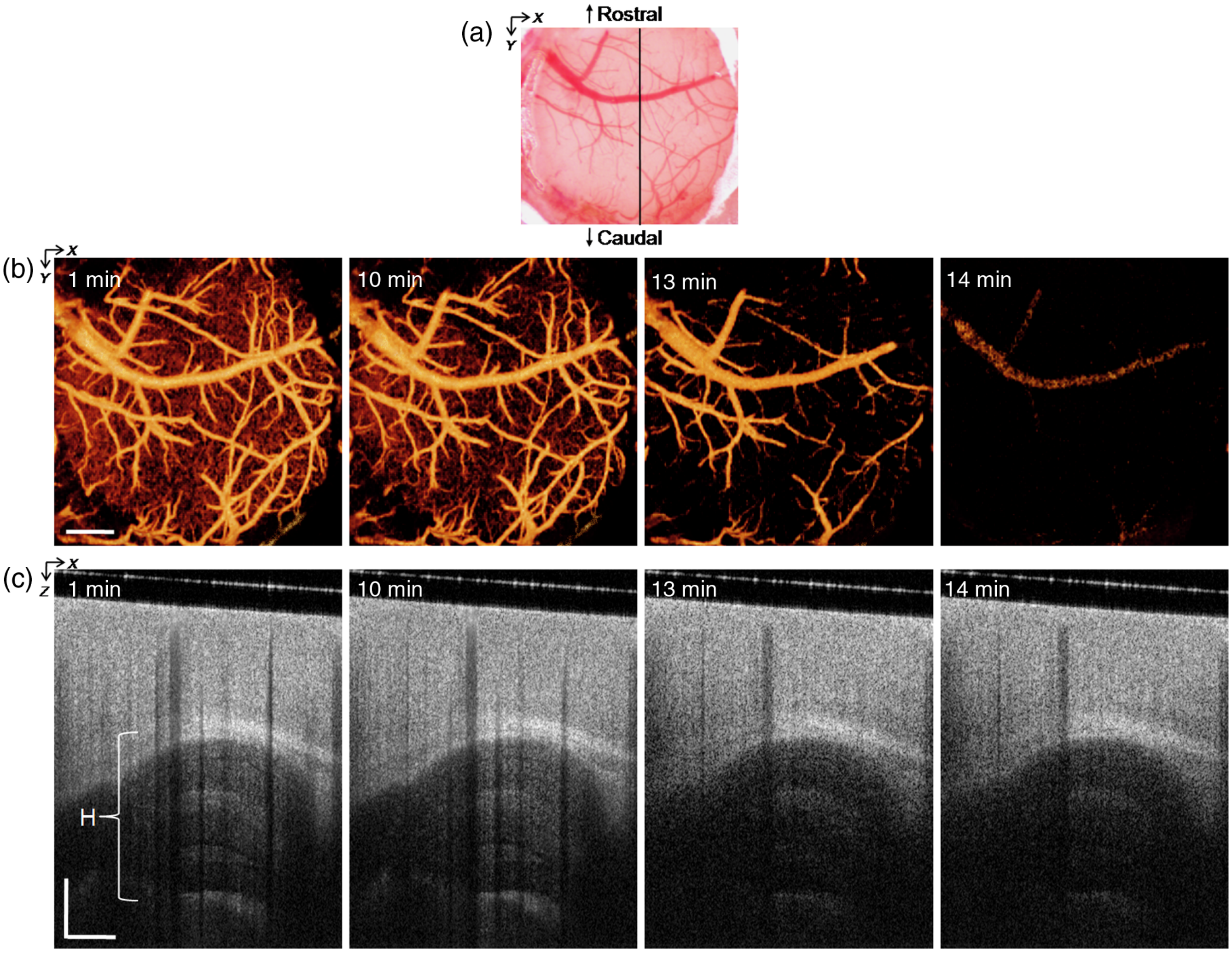

Fig. 4 Time-lapse observation of cerebral change in a cranial window during mouse euthanasia. The cranial window was created in a 10-week-old mouse. For the euthanasia, the mouse inhaled 5% isoflurane overdose and 1 L/min air. (a) Bright-field microscope image of the cranial window. (b) Optical microangiography images of the cerebral cortex in the cranial window showing cessation of blood perfusion at capillaries and small branch vessels 13 min after the inhalation of isoflurane, expanded to all vessels 1 min later. (c) VCSEL SS-OCT images at a sagittal section (a solid line) in the cranial window (a), exhibiting overall OCT signal reduction over the brain structure from 10 min later. H, hippocampus. Scale bar: 500 μm.

Fourier-domain mode locking (FDML) laser[13] whose spectral bandwidth was 110 nm at −3 dB. For this experiment, a 5-week-old young adult mouse with cranial window preparation was used and sequentially imaged with two OCT systems (VCSEL SS-OCT and FDML SS-OCT). For a fair comparison, all OCT systems used the same 5× objective lens (LSM03) and the same scanning protocol for imaging: a B-scan consisting of 400 A-lines and 400 B-frames for the C-scan, covering a scanned area of 3 mm × 3 mm. During imaging, the position of the focal spot was kept the same at ∼500 μm below the brain surface, and each OCT imaging session was completed within 15 min. Moreover, all the OCT images were scaled with the same logarithmic range. The average optical power of the incident beam was 15 and 7 mW for the FDML SS-OCT system and the VCSEL SS-OCT system, respectively. The measured sensitivity (in air) of the FDML SS-OCT system was 102.63 dB at the focus depth position and had ∼3-dB sensitivity loss at 2-mm depth, as shown in Fig. 3(d).

The imaging results are described in Fig. 3. Figure 3(a) shows a bright-field microscope image of the cranial window, and Figs. 3(b) and 3(c) represent an FDML SS-OCT image and VCSEL SS-OCT image, obtained at a coronal section marked by a solid line in the cranial window [Fig. 3(a)], respectively. The cerebral cortex and the corpus callosum just below the cortex are clearly visible in all the SS-OCT images, whereas the observation of brain structures beyond the cortex is only possible with the VCSEL SS-OCT image [Fig. 3(c)]. The deep brain structures are apparent in VCSEL SS-OCT images at different locations of the brain [Fig. 3(f)], while no structures are seen below the cortex for the corresponding FDML SS-OCT images [Fig. 3(e)]. This demonstrates significant improvement in imaging depth of the proposed approach in comparison to conventional SS-OCT systems for mouse brain imaging. Here, the results are given using a wavelength of 1.3 μm. It is known that the light scattering is reduced with the increase of the wavelength.[14] It therefore would be expected that the use of longer wavelengths beyond 1.3 μm could give additional benefits for OCT deep brain imaging but may be compromised with increased optical absorption by water content (>77%) in the brain tissue.[15]

3.3 Observation of Cerebral Change During Euthanization

As a simple imaging application to utilize the proposed approach, we monitored the change in brain structure during euthanasia after the terminal experiment. The experiment was conducted on a 10-week-old adult mouse with inhalation of 5% isoflurane overdose and 1 L/min air while OCT brain imaging was continuously performed over time. To observe additional cerebrovascular behavior, we employed an OCT angiography (OCTA) technique,[16,17] especially an intensity-based optical microangiography (OMAG)[18] because of phase instability of the current VCSEL SS-OCT system. The OCTA can offer simultaneous tissue tomography and functional vessel information within the tissue without a need for contrast agents.[16] Figures 4(b) and 4(c) show time-lapse changes in cerebral structures and vasculatures in the cranial window [Fig. 4(a)] over 14 min of the euthanasia process, respectively. In the OMAG images [Fig. 4(b)], blood perfusions of all capillaries and small branch vessels in the cortex were ceased 13 min after the isoflurane inhalation (the mouse appeared to be euthanized), and no microcirculation for all vessels was observed at 14 min (low signals in the vein may be due to Brownian motion of red blood cells). Meanwhile, the OCT images in Fig. 4(c) [taken from a sagittal section (a solid line) in Fig. 4(a)] show overall OCT signal reduction over the brain structures for a few minutes right after the euthanasia, especially noticeable at the hippocampal region (H).

4 Conclusion

We have demonstrated the feasibility of noninvasive, *in vivo* deep brain imaging of small rodent models using the 1.3-μm VCSEL-based SS-OCT system. We have shown that this OCT system is able to offer remarkable signal sensitivity advantages, experimentally measured at 105 dB constant over a depth of 4.25 mm, providing an extended imaging depth range of more than 2 mm in highly scattering biological samples. The OCT measurements of open-skull cranial window models of adult mice have allowed for the visualization of the cerebral cortex as well as deeper brain structures such as the hippocampus at a depth up to 2.3 mm. This OCT approach to brain study using mouse models would promise to examine morphological or possible functional alterations in both normal physiologies, such as aging and diseased states, such as dementia, Alzheimer's disease, and brain tumors, of the hidden brain tissue. In doing so, the system would be capable of monitoring either acute or longitudinal changes in them *in vivo* due to its minimally invasive procedure.

Acknowledgments

The work was supported in part by National Institutes of Health grants (R01HL093140 and R01EB009682).

References

1. A. M. Zysk et al., "Optical coherence tomography: a review of clinical development from bench to bedside," *J. Biomed. Opt.* **12**(5), 051403 (2007).
2. V. J. Srinivasan et al., "Optical coherence microscopy for deep tissue imaging of the cerebral cortex with intrinsic contrast," *Opt. Express* **20**(3), 2220–2239 (2012).
3. Y. Chen et al., "Optical coherence tomography (OCT) reveals depth-resolved dynamics during functional brain activation," *J. Neurosci. Methods* **178**(1), 162–173 (2009).
4. Y. Jia et al., "Label-free in vivo optical imaging of functional microcirculations within meninges and cortex in mice," *J. Neurosci. Methods* **194**(1), 108–115 (2010).
5. I. Grulkowski et al., "High-precision, high-accuracy ultralong-range swept source optical coherence tomography using vertical cavity surface emitting laser light source," *Opt. Lett.* **38**(5), 673–675 (2013).
6. I. Grulkowski et al., "Retinal, anterior segment and full eye imaging using ultrahigh speed swept source OCT with vertical-cavity surface emitting lasers," *Biomed. Opt. Express* **3**(11), 2733–2751 (2012).
7. W. J. Choi et al., "In vivo imaging of functional microvasculature within tissue beds of oral and nasal cavities by swept-source optical coherence tomography with a forward/side-viewing probe," *Biomed. Opt. Express* **5**(8), 2620–2634 (2014).
8. J. Binding et al., "Brain refractive index measured in vivo with high-NA defocus-corrected full-field OCT and consequences for two-photon microscopy," *Opt. Express* **19**(6), 4833–4847 (2011).
9. "The maximal allowed cw-powers for the laser classes 1, 2, 3R and 3B according to the standard EN 60825-1:2007," 2012, https://en.wikipedia.org/wiki/Laser_safety#/media/File:Laser_class_EN_60825-1.en.png
10. A. Ahmad et al., "Real-time in vivo computed optical interferometric tomography," *Nat. Photonics* **7**(6), 444–448 (2013).
11. K.-S. Lee et al., "Bessel beam spectral-domain high-resolution optical coherence tomography with micro-optic axicon providing extended focusing range," *Opt. Lett.* **33**(15), 1696–1698 (2008).
12. "Allen Brain Atlas," http://mouse.brain-map.org/

13. Z. Zhi et al., "4D optical coherence tomography-based micro-angiography achieved by 1.6-MHz FDML swept source," *Opt. Lett.* **40**(8), 1779–1782 (2015).
14. U. Sharma et al., "Long-wavelength optical coherence tomography at 1.7 μm for enhanced imaging depth," *Opt. Express* **16**(24), 19712–19723 (2008).
15. G. M. Hale et al., "Optical constants of water in the 200 nm to 200 μm wavelength region," *Appl. Opt.* **12**(3), 555–563 (1973).
16. R. K. Wang et al., "Three dimensional optical angiography," *Opt. Express* **15**(7), 4083–4097 (2007).
17. R. K. Wang et al., "Mapping of cerebrovascular blood perfusion in mice with skin and cranium intact by optical micro-angiography at 1.3 μm wavelength," *Opt. Express* **15**(18), 11402–11412 (2007).
18. Y. P. Huang et al., "Swept-source OCT angiography of the retinal vasculature using intensity differentiation based OMAG algorithms," *Ophthalmic Surg. Lasers Imaging Retina* **45**(5), 382–389 (2014).